

1. Background

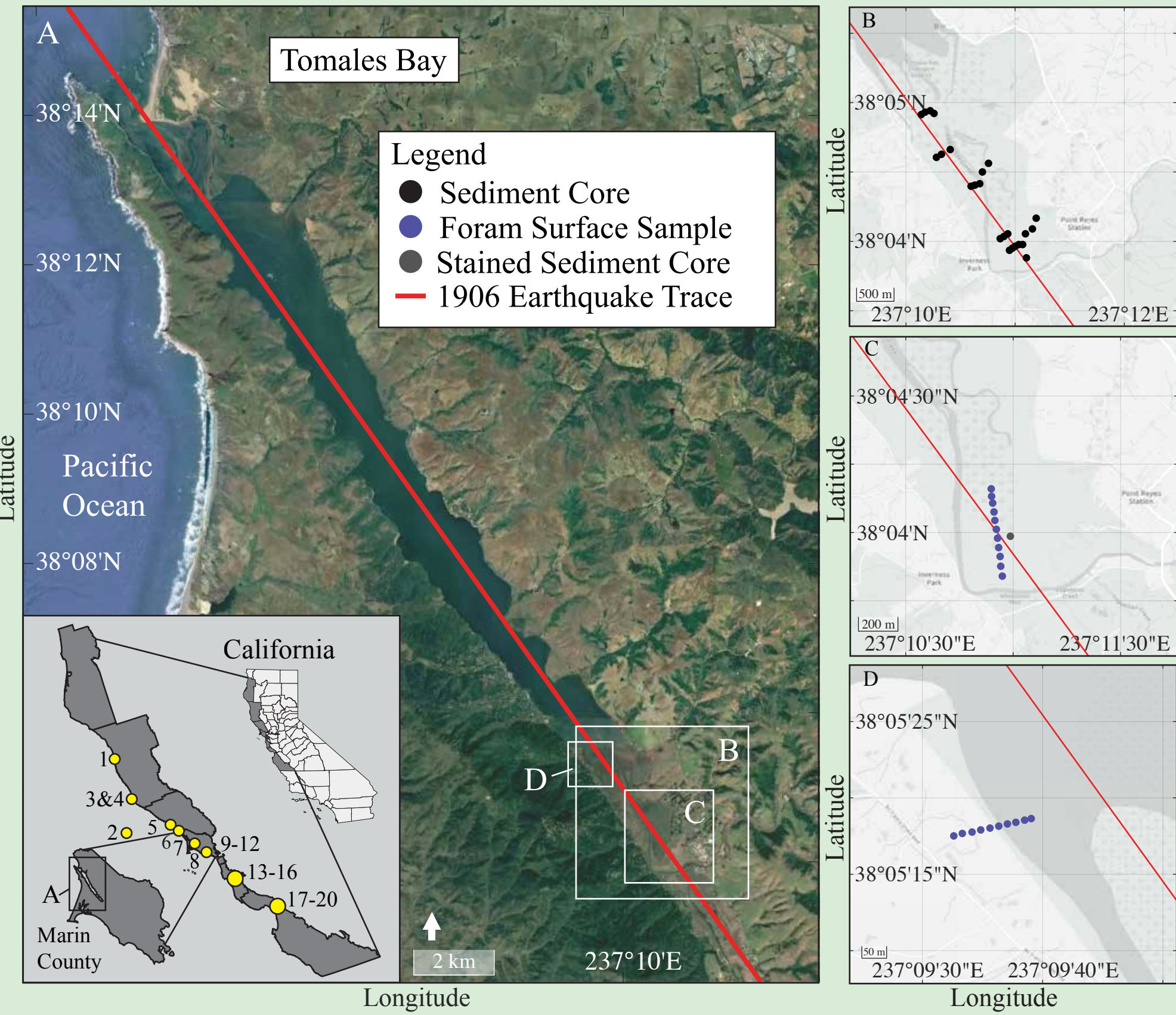
The 1906 San Francisco earthquake caused coseismic subsidence in marshes of upper Tomales Bay, which lies within the San Andreas Fault zone. These marsh deposits may preserve a long-term record of past earthquakes along the Northern San Andreas Fault.

2. Research Questions

- 1) Can we use stratigraphy paired with a foraminifera-based transfer function to detect abrupt vertical changes in marsh stratigraphy along a strike slip fault?
- 2) Do the identified subsidence horizons align with other independent earthquake records along the San Andreas Fault system?
- 3) What is the recurrence interval of throughgoing ruptures on the Northern San Andreas Fault over the last 4,000 years?

3. Study Area

43 cm of subsidence was recorded in Tomales Bay's southern delta after the 1906 SF earthquake (Lawson, 1908).



A location inland from the open ocean and high sedimentation rate give Tomales Bay the potential to preserve records of paleoseismicity.

Figure 1: A) Study area of Tomales Bay showing location of the 1906 earthquake trace in red. Numbers on inset refer to previous paleoseismic study locations, detailed in figure 6. B) Sediment core locations. C&D) Modern foraminifera transect locations.

4. Methods

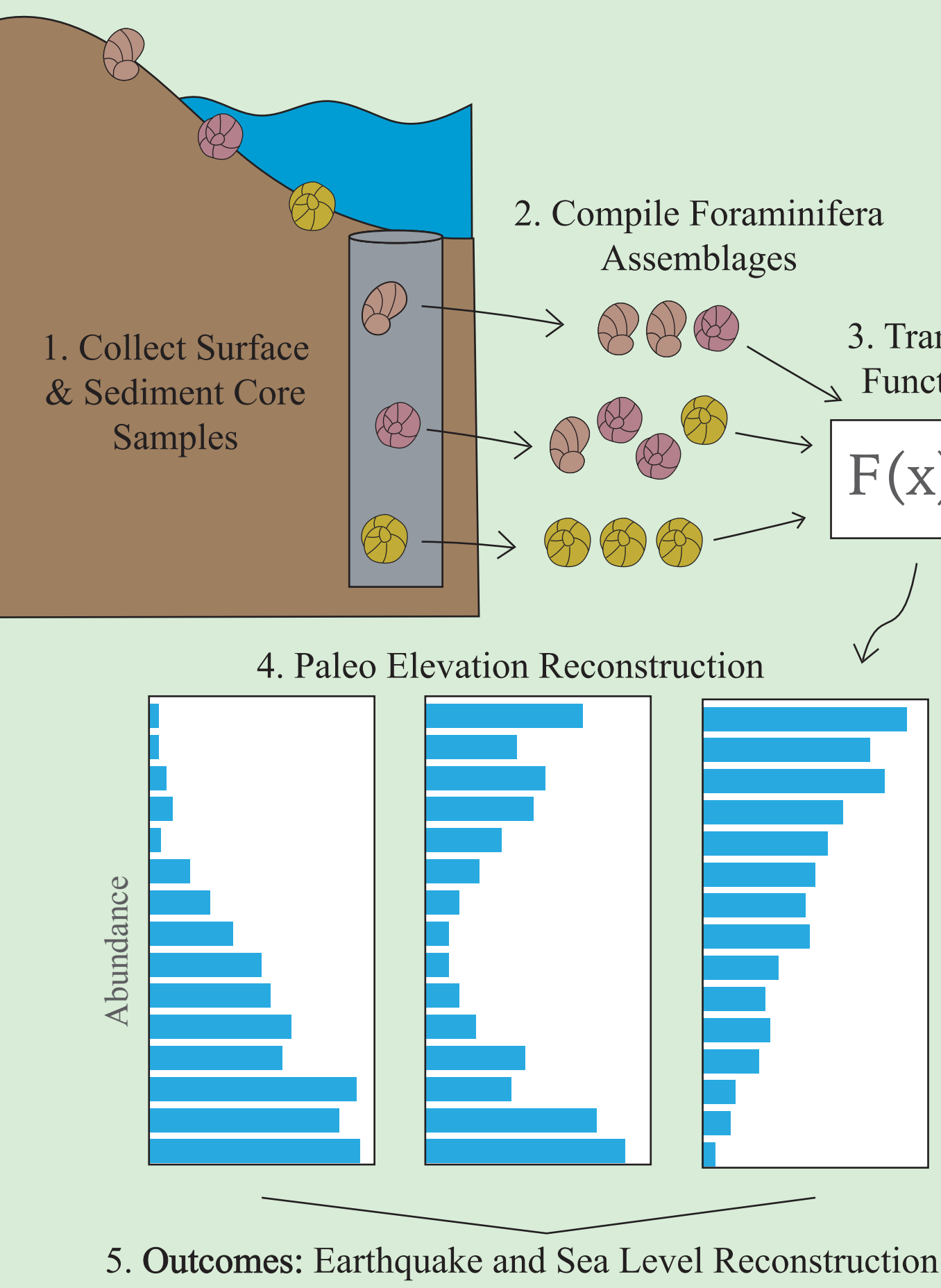


Figure 2: Schematic workflow of how to set up a transfer function using surface and fossil foraminifera.

To answer our research questions, we used:

Sediment Cores
-Collected 26 Vibracores from 0.5m - 4m in length to examine stratigraphy, looking for sharp sedimentary contacts.

Radiocarbon Dating
-53 radiocarbon ages (articulated bivalve, gastropod shells, and wood fragments) were collected to date candidate events
-Radiocarbon ages were measured at the University of California Irvine Keck carbon cycle accelerator mass spectrometry (KCCAMS) facility.

Foraminifera
-Surveyed modern foraminifera distributions at 2 elevational transects to build a reference dataset
-Applied a Bayesian transfer function to fossil assemblages within sediment cores for paleoenvironmental reconstructions across contacts of interest.

5. Results

- Two clusters of modern foraminifera assemblages composed of 10 species were found.

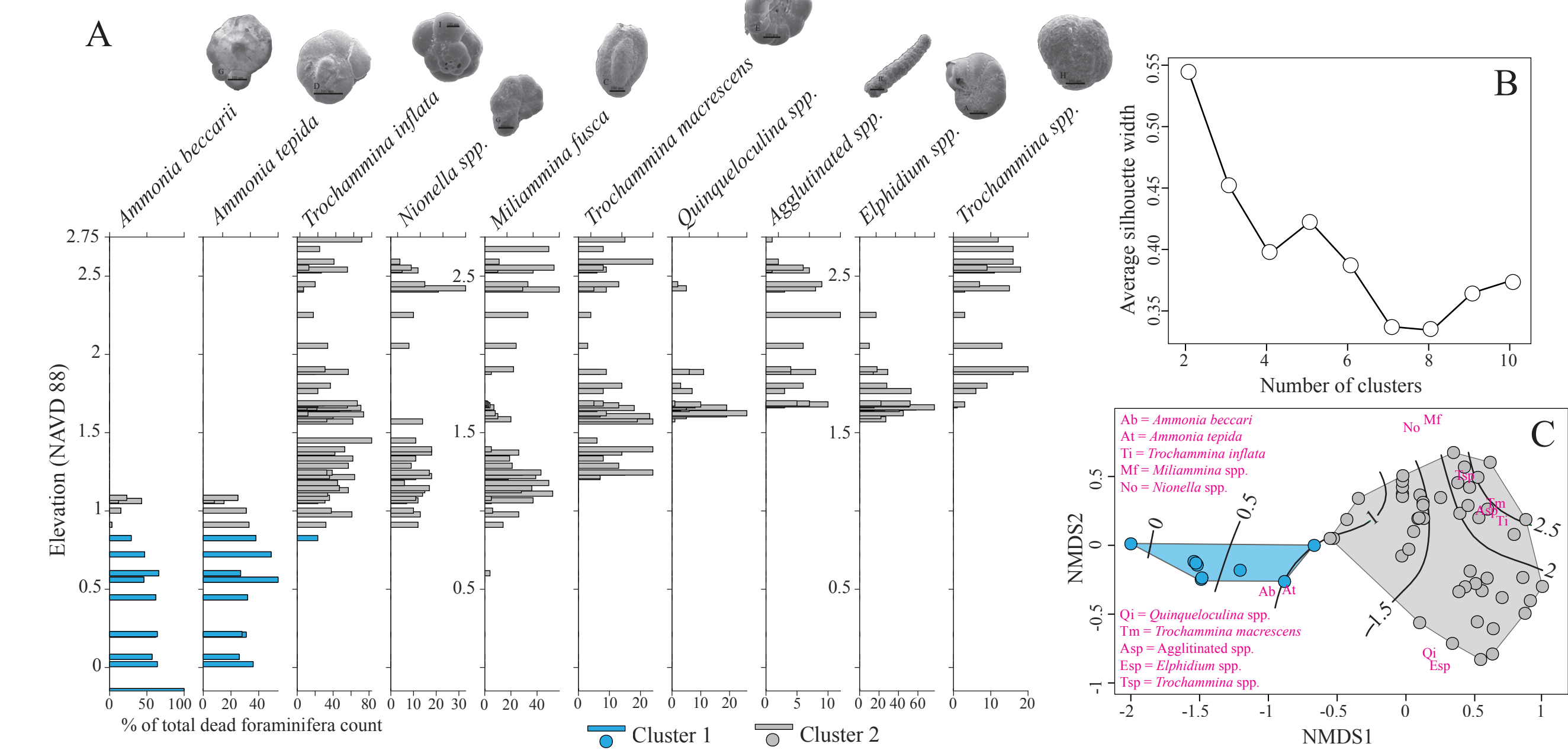


Figure 3: A) Modern foraminifera assemblages plotted with relative abundance of each species on the x axis, and elevation with respect to NAVD 88 on the y axis. SEM image of each species above species name if available. Color represents cluster 1 (blue) and cluster 2 (grey). B) Average PAM silhouette width with increasing numbers of clusters. We select two clusters to maximize the average width. C) Non-metric multidimensional scaling (NMDS) sample plot with elevation contours (NAVD-88) passively projected.

- Four main sedimentary facies were identified, as well as 5 sharp contacts within 3 core transects.

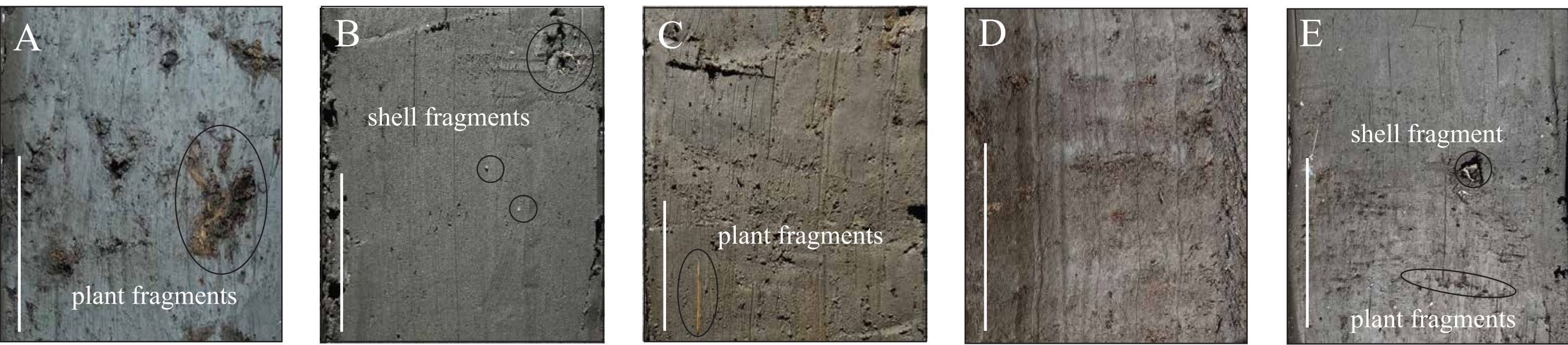


Figure 4: Sediment facies. A: Organic rich mud (ORM) facies, TB21-13; B: Organic poor mud (OPM) facies, TB21-14; C: Modeled organic mud facies, TB21-14; D: Interlaminated mud facies, TB22-02; E: Event 3 contact, TB21-15.

- Fossil foraminifera were picked above and below each contact of interest, and a Bayesian transfer function was used to create a paleoenvironmental reconstruction for each contact.

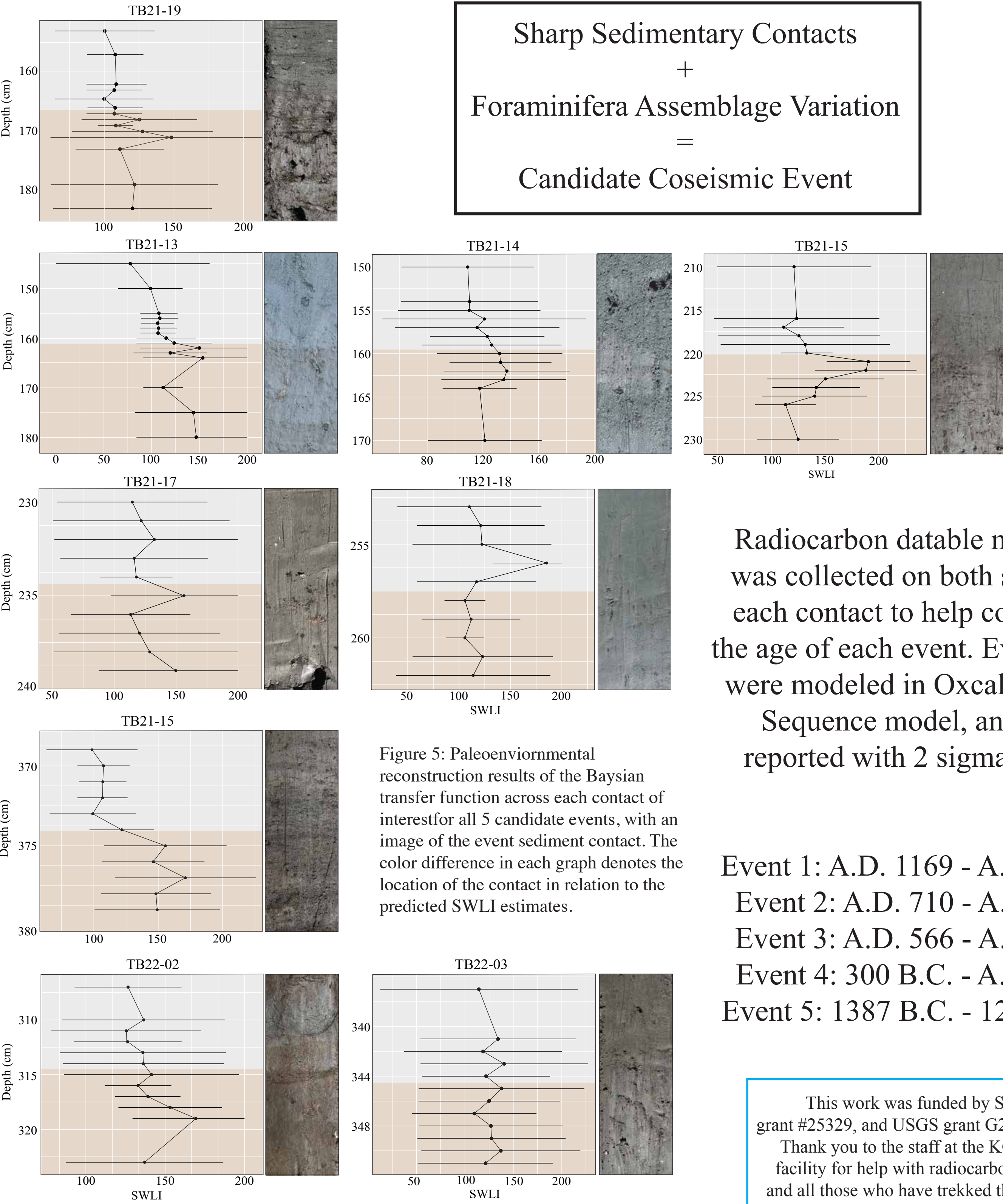


Figure 5: Paleoenvironmental reconstruction results of the Bayesian transfer function across each contact of interest for all 5 candidate events, with an image of the event sediment contact. The color difference in each graph denotes the location of the contact in relation to the predicted SWLI estimates.

Radiocarbon datable material was collected on both sides of each contact to help constrain the age of each event. Event ages were modeled in Oxcal using a Sequence model, and are reported with 2 sigma error.

- Event 1: A.D. 1169 - A.D. 1370
- Event 2: A.D. 710 - A.D. 862
- Event 3: A.D. 566 - A.D. 630
- Event 4: 300 B.C. - A.D. 171
- Event 5: 1387 B.C. - 1297 B.C.

This work was funded by SCEC grant #25329, and USGS grant G21AP10385. Thank you to the staff at the KCCAMS facility for help with radiocarbon dating, and all those who have trekked through the mud with me to collect cores and forams!

*Events 3 and 5 display a sharp sedimentary contact but had poor foraminiferal preservation. Thus, although the sedimentary nature of the contact suggests subsidence, the large errors in the transfer function do not allow for a definitive interpretation.

6. Event Timing

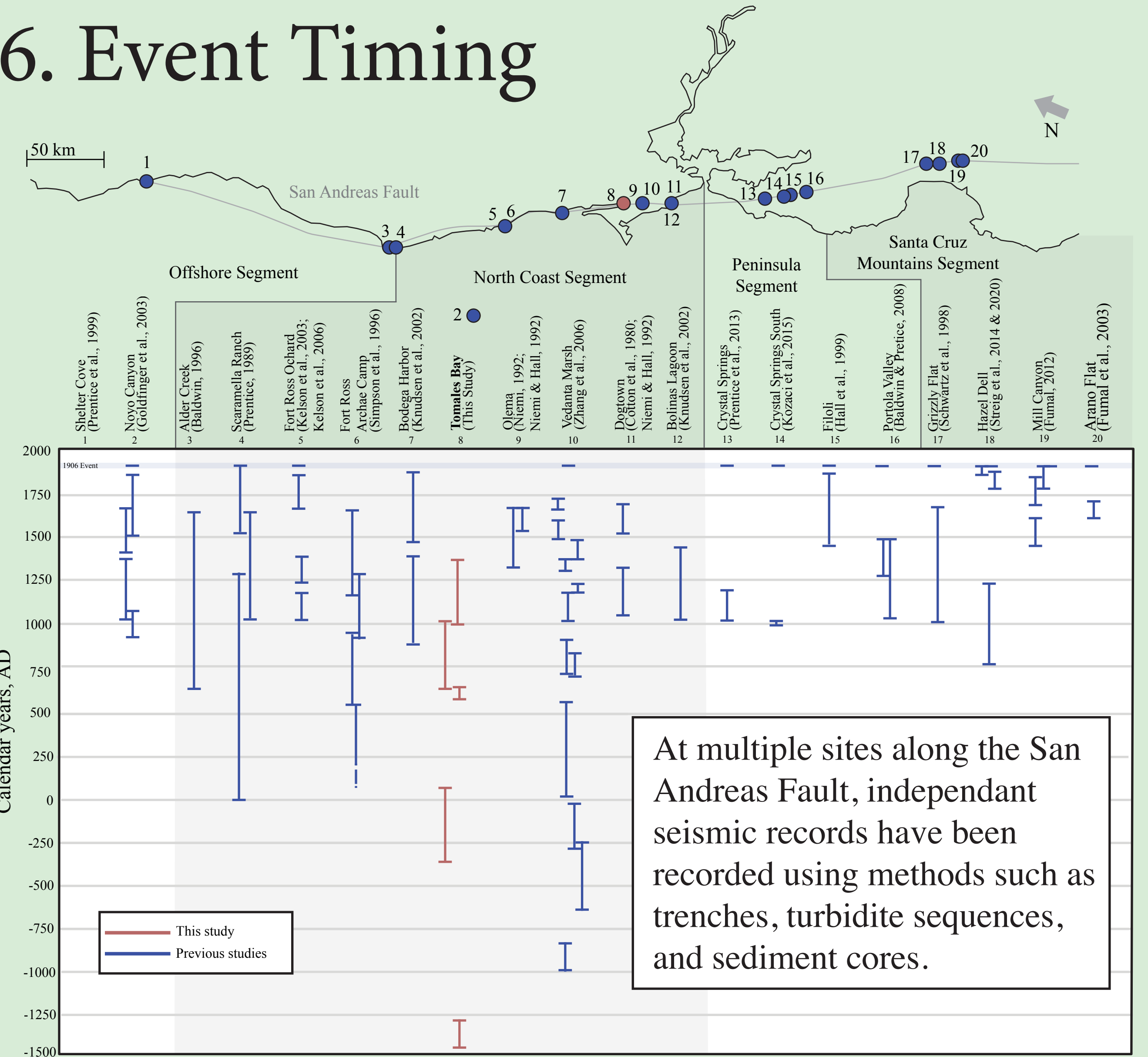


Figure 6: Space-time diagram for the Northern SAF with study locations. Vertical bars represent calibrated age limits for surface rupture events based on minimum and maximum limiting radiocarbon age estimates.

To better understand if some of these records may be evidence of throughgoing ruptures of the North Coast segment, we recalibrated and modeled age estimates for 7 studies, and clustered events based on overlap quantity of each earthquake's probability density function (PDF). Due to the confidence in the occurrence of a ~1600 A.D. event, we choose an overlap of 26% as our cluster cutoff.

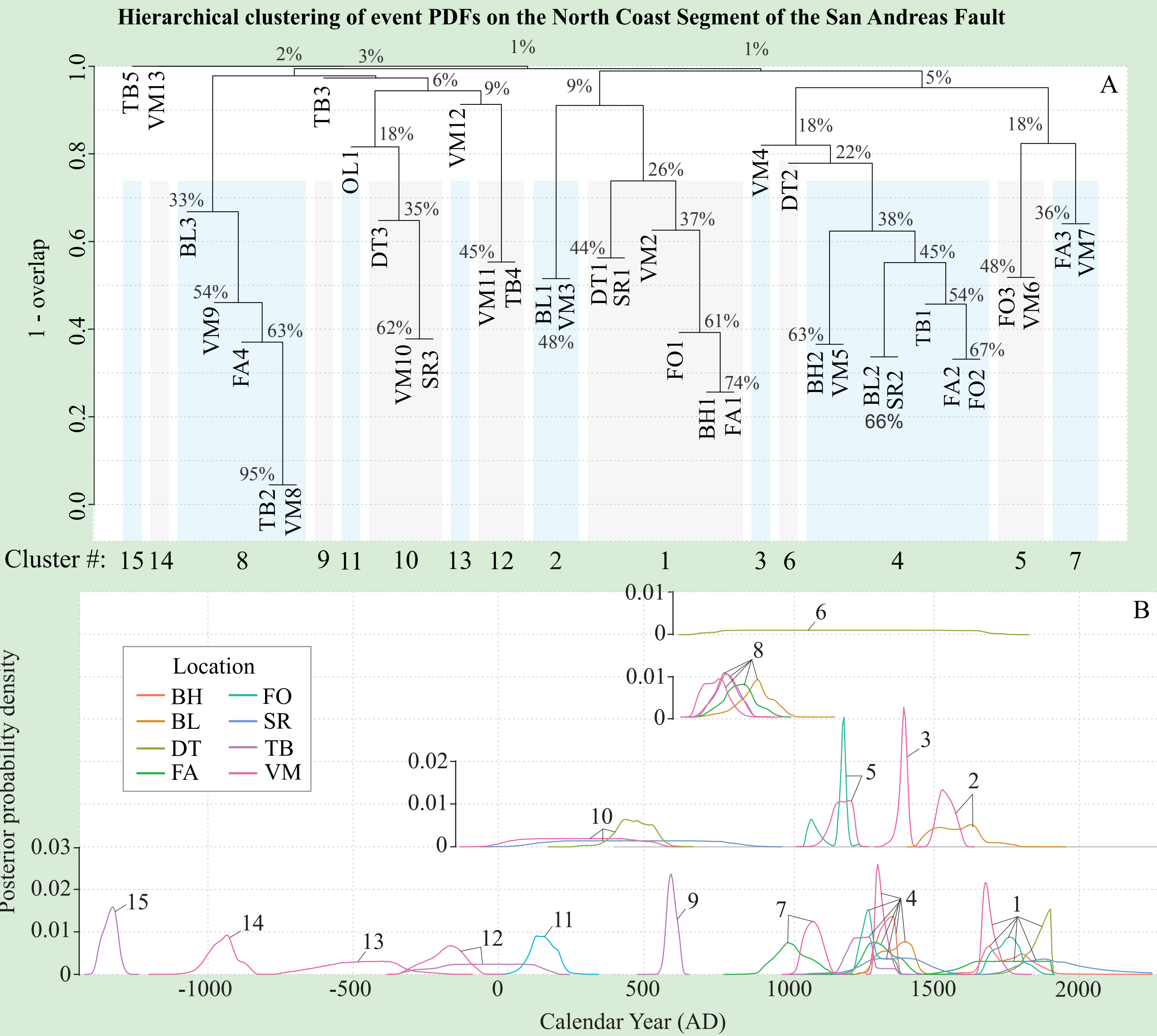


Figure 7: A) Hierarchical clustering dendrogram of earthquake-event PDFs from multiple locations. Pairwise similarity between event PDFs was quantified as the integral of their overlap (0 = no overlap, 1 = complete overlap). Distances for clustering are defined as 1 - overlap, so branches that join at lower heights indicate events with greater similarity in their age probability distributions. The y-axis shows this distance metric, while the x-axis lists individual event-location PDFs, and shows the cluster they are assigned to using a 26% similarity cutoff. B) PDFs for each earthquake event recorded along the North Coast Segment, colored by location. Tiering of clusters is done to more clearly see overlap. Numbers refer to cluster groups from panel A. BH - Bodega Harbor; BL - Bolinas Lagoon; DT - Dogtown; FA - Fort Ross Archæ; FO - Fort Ross Orchard; SR - Scaramella Ranch; TB - Tomales Bay; VM - Vendanta Marsh

With this method, we separated out 15 individual events, 4 of which were recorded at 3 or more sites. These give us mean estimates of A.D. 1600, A.D. 1300, A.D. 700, and A.D. 400 for throughgoing ruptures, reinforcing a 300 year recurrence interval.